frontiers | Frontiers in Earth Science

TYPE Original Research
PUBLISHED 21 August 2023
DOI 10.3389/feart.2023.1216614

OPEN ACCESS

EDITED BY
Xuelong Li,
Shandong University of Science and Technology, China

REVIEWED BY
Danqing Song,
South China University of Technology, China
Cai Ziyong,
Central South University, China
Xiangfeng Guo,
National University of Singapore, Singapore

*CORRESPONDENCE
Zhao Yang,
45574335@qq.com

RECEIVED 04 May 2023
ACCEPTED 07 August 2023
PUBLISHED 21 August 2023

CITATION
Liu P, Sun S, Yang Z, Ji F, Xu C and Zhu H (2023), Impact of anti-sticking coating technology on shear strength at the clay-metal interface in cohesive strata. *Front. Earth Sci.* 11:1216614. doi: 10.3389/feart.2023.1216614

Impact of anti-sticking coating technology on shear strength at the clay-metal interface in cohesive strata

Pengfei Liu[1], Shicheng Sun[2], Zhao Yang[1]*, Fuquan Ji[1], Chao Xu[1] and Hanbiao Zhu[3]

[1]CCCC Second Harbor Engineering Company Ltd., Wuhan, China, [2]CCCC First Harbor Engineering Company Ltd., Tianjin, China, [3]School of Civil Engineering, Central South University, Changsha, China

The shield machine is clogged frequently when tunneling in cohesive strata. Shield clogging is closely linked to the shear strength exhibited at the clay-metal interface. To investigate the impact of anti-sticking coating technology on the shear strength at the clay-metal interface, a series of direct shear tests were conducted. The obtained test results revealed an initial increase in shear stress at the clay-metal interface as shear displacement increased, eventually reaching a state of stabilization. The shear strength exhibited a gradual increase initially, followed by a significant increase, and eventually reached a plateau with the rise in the consistency index. It was observed that the adhesion between the anti-adhesion coating and clay was relatively weak, but the presence of the anti-adhesion coating effectively reduced the risk of shield clogging.

KEYWORDS

shield tunneling, cohesive strata, tunnel excavation, anti-adhesion coating, shield clogging

1 Introduction

Currently, China has emerged as the leading country worldwide in terms of scale and complexity of tunnel and underground construction (Song et al., 2021; Xu et al., 2022). The 21st century has witnessed significant advancements in underground engineering in China (Ding and Xu, 2017; Liu et al., 2020; Huang et al., 2022). Over the past two decades, numerous tunnels have been successfully constructed (Wang et al., 2022a; Zhou et al., 2022; Wang et al., 2023a). The shield tunneling technology, known for its safety and efficiency, has been extensively utilized in the construction of urban subways and municipal tunnels (Langmaack and Lee, 2016; Xu et al., 2020; Jia and Gao, 2022). However, when a shield machine traverses clayey strata, the excavated clayey muck tends to adhere to the cutter head and cutters (Hollmann and Thewes, 2013; Wang et al., 2023b; Gao et al., 2023). The force exerted during shield pushing causes the attached muck to consolidate, resulting in the formation of a layer of hardened muck on the surface of cutter head (Thewes and Hollmann, 2016; Zeng et al., 2020; Li et al., 2021). As the hard muck rubs against the ground, heat is generated at the tunneling face. This heat accelerates the consolidation of muck adhering to the steel instruments. Consequently, the cutter becomes completely engulfed in consolidated muck, rendering it incapable of cutting and leading to a clogging in the shield machine. The shield clogging can have various adverse effects. In milder cases, it can lead to a loss of cutting efficiency of the cutting tools, significantly impacting the tunneling construction efficiency.

In more severe instances, it can cause surface subsidence, posing risks to surface structures and personnel safety. For example, a large diameter shield tunneling machine was clogged when it was passing through a railway station in Shenzhen, China. The on-site construction personnel used frequent cabin cleaning to remove the soil adhered on the cutter head, resulting in a significant increase in ground settlement and settlement rate, posing a huge threat to the safety of surface railway station.

Based on current engineering experience, both slurry pressure balance (SPB) and Earth pressure balance (EPB) shields can face clogging issues in clayey strata (Chen et al., 2022; Li et al., 2022). To mitigate shield clogging during EPB tunneling, soil conditioning chemicals are frequently injected ahead of the cutter head (Martinelli et al., 2015; Zumsteg and Langmaack, 2017; Liu et al., 2018; Wang et al., 2021). However, the injection holes for soil conditioning chemicals in the cutter head are sparsely distributed, making it challenging to evenly distribute the injected chemicals across the entire cutter head. Consequently, certain areas may still experience shield clogging. During SPB shield tunneling, the central position of the cutter head is washed with slurry sprayed from the pipeline to prevent muck adhesion (Xiao et al., 2020). Nevertheless, due to limited flow rates, the cutter head may still encounter clogging issues in cases of high adhesion strata or poorly designed cutter heads (Yang et al., 2023).

Shield clogging is primarily caused by the strong adhesive strength between metal and clay, also known as the clay-metal interface strength (Sass and Burbaum, 2009; Wang et al., 2020; Liu et al., 2022). The clay-metal interface strength can be divided into the normal direction perpendicular to the contact and the tangential direction along the interface (Zumsteg et al., 2013; Burbaum and Sass, 2017; Li et al., 2023). The cutting tool used in shield tunneling tears through the stratum, with the muck predominantly flowing tangentially along the cutter head. When the tangential strength, referred to as the shear strength of the clay-metal interface, is too high, it causes the flow of muck to halt and results in shield clogging. Therefore, the shear strength of the clay-metal interface is the primary factor contributing to shield clogging (Zumsteg and Puzrin, 2012; Liu et al., 2018; Liu et al., 2019). Several researchers have conducted relevant studies on the shear strength of the clay-metal interface. Zumsteg and Puzrin (2012) developed a rotating shear device to evaluate the shear strength between metal and clay in the interface. They investigated the impacts of metal surface roughness, water content, and applied pressure on the soil specimen. The findings demonstrated that an increase in surface roughness or normal pressure applied to the soil specimen led to a steady increase in the shear strength of the clay-metal interface. However, the shear strength dramatically decreased as the water content rose. Basmenj et al. (2016) used a direct shear apparatus and inserted the bottom half of the shear box into a metal block to test the shear strength of the clay-metal interface. They analyzed the variation in shear strength for soil specimens with different clay contents using the consistency index. The results showed that when the consistency index was low, the shear strength of the clay-metal interface remained relatively constant, but it increased rapidly when the consistency index surpassed a certain threshold. Bircha et al. (2016) investigated the relationship between water content, compactness, and the fluctuation of shear strength between sand, silt, clay, and metal. The study demonstrated that the shear strength of the clay-metal interface initially increased and subsequently decreased as the water content increased. Furthermore, the shear strength of the clay-metal interface decreased with the level of sand and silt compactness. Wang et al. (2022b) investigated the effects of the consistency index, normal pressure, clay plasticity, contact angle, and metal surface roughness on the shear strength of the clay-metal interface. They found that normal pressure, consistency index, and hydrophilicity of the metal surface significantly influenced the shear strength. In shield tunneling, the normal pressure is related to the tunnel face support pressure. Lower face support pressure reduces the likelihood of shield clogging but may lead to tunnel face collapse (Cao et al., 2020; Wang et al., 2022c; Niu et al., 2022). Therefore, simply decreasing the normal pressure is not a viable solution to avoid shield clogging. The natural water content and Atterberg limits of the soil in the stratum, which are challenging to modify, determine the consistency index. By applying an anti-adhesion substance to cover the cutter head and cutter, it is possible to reduce the hydrophilicity of the metal surface and prevent shield clogging. Preventing the formation of shield clogging can significantly improve shield tunneling construction efficiency and eliminate construction risks in cohesive strata. Coating technology is widely employed in various industries. For instance, in the medical field, anti-adhesion substances are coated on the surface of medical devices to reduce bacterial adhesion (Yang et al., 2022). In the glass manufacturing industry, anti-adhesion coatings are used to enhance the surface roughness of products by applying them to the mold surface (Zhang et al., 2020). Similarly, coatings are utilized to prevent corrosion in offshore wind power plants (Eom et al., 2020). However, there has been limited recent research specifically focusing on the application of anti-adhesion coatings to address shield clogging in tunnel engineering.

To investigate the impact of anti-adhesion coating on preventing shield clogging, this study conducted a comprehensive series of direct shear tests to measure the shear strength of the clay-metal interface under varying water contents. The analysis focused on examining the influence of the consistency index on the shear strength of the clay-metal interface and comparing the shear strength with and without the application of an anti-adhesion coating. The results confirmed the effectiveness of the anti-

TABLE 1 Mineral composition of the soil specimen.

Mineral name	Mass percentage (%)
Albite	46.7
Kaolinite	27.8
Microcline	11.1
Illite	8.3
Montmorillonite	4.4
Calcite	1.6

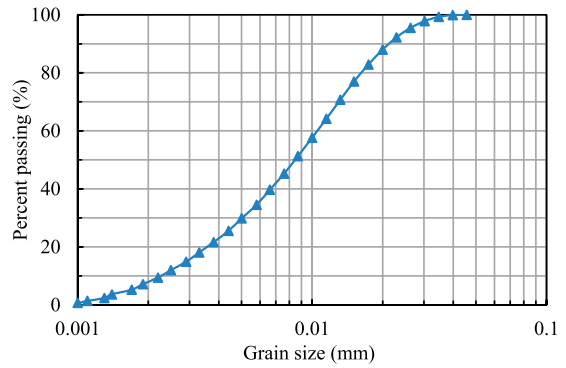

FIGURE 1
Soil gradation curve.

FIGURE 2
Large-scale direct shear apparatus.

adhesion coating and provided further insights into its underlying mechanism.

2 Testing material and scheme

2.1 Testing material

The soil sample used in this study was obtained from a construction site in Wuhan, China. Table 1 presents the results of an X-ray diffraction (XRD) analysis conducted to identify the soil minerals. The analysis revealed the presence of albite, kaolinite, microcline, and small amounts of illite, montmorillonite, and calcite in the soil. The grain size distribution curve was determined using a laser particle size analyzer, as shown in Figure 1. The largest particle size observed was 0.046 mm. The Atterberg limits of the soil specimen were measured using the falling cone method in accordance with the Standards for Geotechnical Test Methods (2019). The liquid limit was determined to be 36.9%, while the plastic limit was found to be 18.9%. The plasticity index, calculated as the difference between the liquid and plastic limits, was 18.0. Since the plasticity index is greater than 17 and more than 50% of the specimen's mass consists of particles smaller than 0.075 mm, the soil specimen is classified as clay according to the USDA. (1938) classification.

2.2 Large-scale direct shear test

Several instruments are used to measure the shear strength of the clay-metal interface, including the soil-metal adapter, static lateral adhesion apparatus, shear plate apparatus, and direct shear apparatus (Zumsteg and Puzrin, 2012; Peila et al., 2015; Basmenj et al., 2016; Bircha et al., 2016). However, there are limitations associated with some of these instruments. For instance, in the static lateral adhesion and soil-metal adapter tests, it is not possible to apply normal pressure on the soil specimen. Additionally, the shear stress on the plate is assumed to be equal, which is clearly unreasonable in the shear plate test. To overcome these limitations, the shear strength of the clay-metal interface was evaluated using a large-scale direct shear apparatus (Figure 2). The testing methodology aligns with that of a typical direct shear device. The direct shear box has dimensions of 15 cm in length and 15 cm in width, with the top and bottom halves of the box each measuring 7.5 cm in height. The soil specimen is placed in the upper section of the box, while the metal block is placed in the lower section. By applying normal pressure to the specimen, the shear strength of the clay-metal interface can be determined.

The metal block was cleaned using alcohol, and after natural drying, an anti-adhesion substance was applied. The metal block was once again dried after spraying the anti-adhesion agent. The hydrophilicity of the metal surface, as indicated by the contact angle, is a key factor influencing the shear strength of the clay-metal interface. The contact angle of water on a solid surface reflects the hydrophilicity of that material. A decrease in the contact angle signifies increased hydrophilicity of the solid material. The water contact angles observed on the coated and untreated metal blocks were 85.48° and 62.04°, respectively.

The large-scale direct shear test involved the following major steps:

(1) The soil samples were dried at 105°C for a minimum of 24 h. Any agglomerated soil was broken using a rubber hammer, ensuring that the soil particles were not damaged. To achieve the desired water content, the dry soil specimen weighing 3 kg was mixed with water and left undisturbed for 24 h to allow complete water absorption.
(2) The lower portion of the direct shear box was filled with the metal block. The upper and lower halves of the box were aligned and securely fixed using clamping screws. The prepared soil specimen was then placed layer by layer in the upper portion of the box until its surface was approximately 1 cm below the top of the box.
(3) The specimen was covered with filter paper and a loading plate. The required normal pressure was applied to the specimen. In this study, the fast shear test, which is an undrained and unconsolidated shear test, was conducted to simulate the

TABLE 2 Large-scale direct shear test conditions.

Anti-adhesion coating	Normal pressure values (kPa)	Water content range (%)	Consistency index (I_c)
Uncoated	100	10–30	0.3–1.6
	200		
Coated	300		
	400		

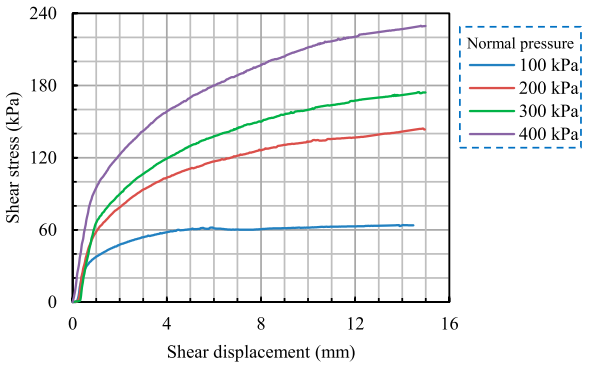

FIGURE 3
Shearing curves between uncoated metal block and clay with 10% water content.

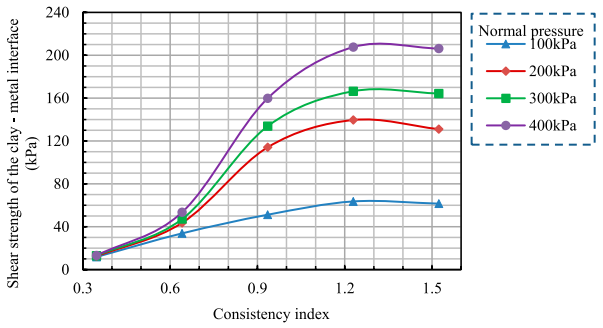

FIGURE 4
Variations in the shear strength between uncoated metal block and clay with the consistency index.

release of muck during shield tunneling without drainage and consolidation.

(4) After applying the necessary pressure, the clamping screws were removed, and the shear test was initiated. The shear stress and displacement were monitored at a frequency of 1 time per second, and the shear rate was set to 1 mm/min, following the Standards for Geotechnical Test Methods.

(5) The measured data were recorded and analyzed after the completion of the shearing process. The actual water content of the soil sample next to the metal block was also measured.

A series of extensive direct shear tests were conducted under various normal pressures to investigate the effect of the anti-adhesion coating on the prevention of shield clogging, as presented in Table 2.

3 Results of the direct shear test

3.1 Shearing curve

Figure 3 illustrates the shearing curves of soil sample with 10% water content obtained from the direct shear testing. Initially, as the shear displacement increased, there was a significant rise in shear stress at the metal-clay interface. As the shear displacement approached the point where the contact between clay and metal was disrupted, the shear stress increased gradually. Finally, the shear stress then reached a relatively constant level. When the difference between five consecutive readings is less than 0.5 kPa, it is considered that the shear stress has reached a stable state. The average shear stress during this stable stage was considered to represent the shear strength of the clay-metal interface.

3.2 Variations in the shear strength of the clay-metal interface with the consistency index at different pressures

Due to the variation in Atterberg limits among different clay types with the same water content, they exhibit different degrees of softness. The consistency index (I_c) takes into account the water content and Atterberg limits of the clay. When the water content is at the liquid limit, the consistency index is 0, whereas it is 1 at the plastic limit. For values between the liquid and plastic limits, the consistency index represents the corresponding degree of softness, ranging from 0 to 1. Thus, the consistency index, as represented by Eq. 1, is a normalized value that characterizes the softness state of clay.

$$I_c = \frac{w_l - w}{I_p} \tag{1}$$

Figure 4 illustrates the variation of shear strength of the clay-metal interface with the consistency index, obtained by converting the water content into the consistency index. Each data point represents the average of two experimental results. When the consistency index was below 0.6, the shear strength of the clay-metal interface was very low. A slight increase in shear strength was observed as the consistency index increased. Notably, a significant increase in shear strength occurred within the consistency index range of 0.6–1.2. Once the consistency index exceeded 1.2, the shear

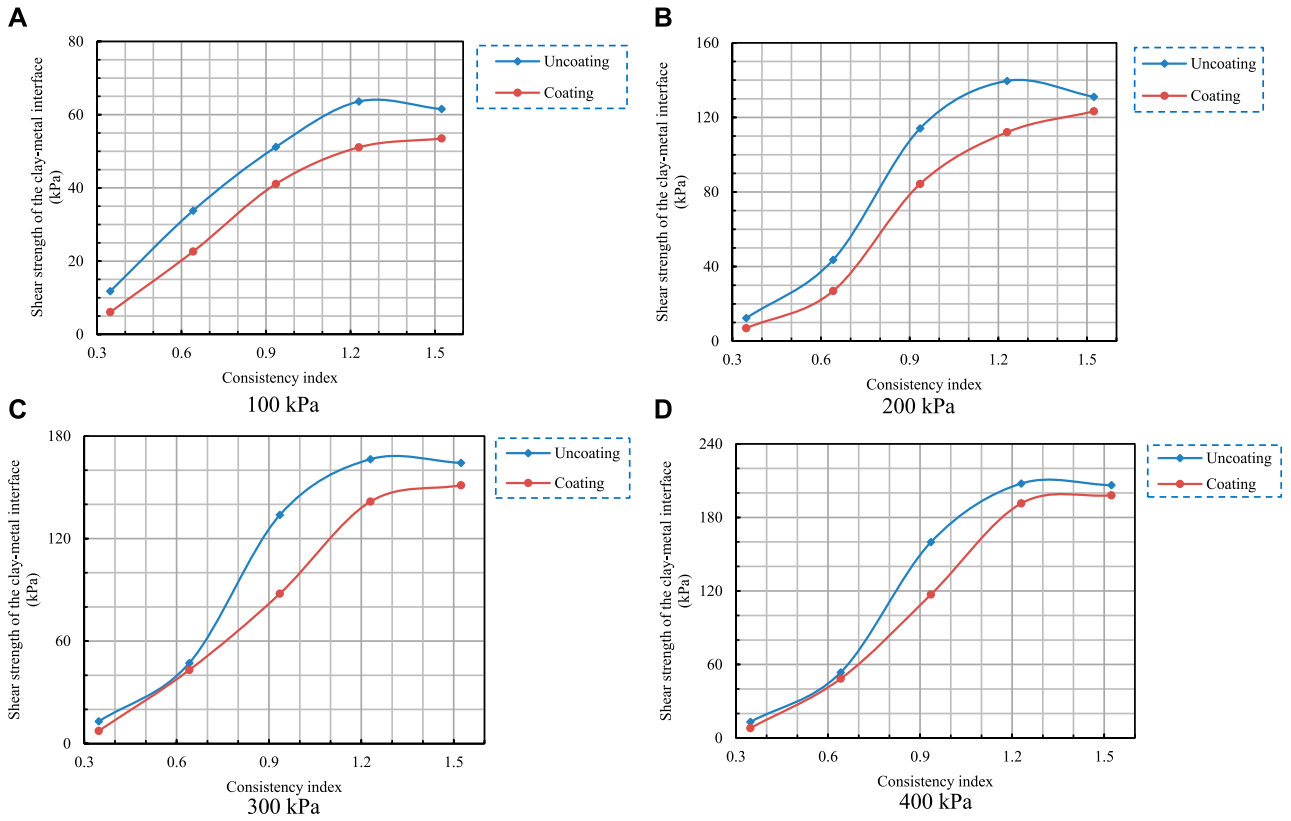

FIGURE 5
Comparison of shear strength between coated or uncoated metal block and clay under normal pressure of **(A)** 100, **(B)** 200, **(C)** 300, and **(D)** 400 kPa.

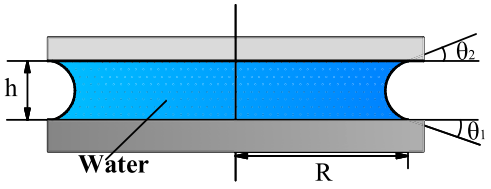

FIGURE 6
Plate-water-plate model.

strength of the clay-metal interface showed minimal variations. Additionally, when the consistency index was below 0.6, there was minimal variation in the shear strength of the clay-metal interface at different normal pressures. However, for consistency indexes above 0.6, the shear strength exhibited a significant increase with increasing normal pressure.

3.3 Effect of anti-adhesion coating on the shear strength of the clay-metal interface

Figure 5 compares the shear strength between coated and uncoated metal blocks and clay at normal pressures of 100, 200, 300, and 400 kPa. The shear strength between the coated metal block and clay exhibited a similar trend to the shear strength between the uncoated metal block and clay, varying with the consistency index. However, the shear strength between the coated metal block and clay was weaker compared to the uncoated metal block under the same consistency index and standard pressure. Furthermore, the difference in shear strength increased as the shear strength of the clay-metal interface increased. The high shear strength of the clay-metal interface, such as the cutter head and cutter, was identified as the primary factor causing shield clogging. The test results showed that the anti-adhesion coating significantly reduced the shear strength of the clay-metal interface. Consequently, the application of an anti-adhesion coating can effectively reduce the likelihood of shield clogging in the adhesive stratum.

4 Discussion on the mechanism of anti-adhesion coating

A water film theory for soil adhesion was proposed by Akiyama and Yokoi. (1972). In this theory, the interaction between clay and the metal block was modeled as a plate-water-plate interface, considering the lamellar structure of clay particles (Ren et al., 1990). This conceptualization is illustrated in Figure 6. The normal force acting on the clay-metal interface is calculated using the Laplace formula (2), which can be expressed as follows (Huang et al., 2013):

$$W = \frac{\pi R^2 \gamma_L (\cos\theta_1 + \cos\theta_2)}{h} \quad (2)$$

where h and R stand for the thickness and radius of the water film, respectively, θ_1 and θ_2 for the metal block and clay's respective contact angles, and γ_L for the water's surface tension. Thus, the following is the tangential force on the clay-metal interface:

$$P = \mu W = \frac{\mu\pi R^2 \gamma_L (\cos\theta_1 + \cos\theta_2)}{h} \quad (3)$$

where the coefficient of friction between the clay and the metal is denoted by μ. According to Eq. 3, the shear strength of the clay-metal interface is inversely proportional to the thickness of the water film (h) and directly proportional to the area of the water film (πR^2). Zhang et al. (2004) reported that as the water content of clay increases from zero to the liquid limit, the water film at the clay-metal interface undergoes three stages: slow increase, rapid growth, and saturation. With an increase in water content or a decrease in consistency, the water film between the clay and metal interface gradually enlarges, leading to an increase in the water film area. Consequently, the shear strength of the clay-metal interface gradually increases during the first stage. When the water content reaches a certain level, the clay-metal interface becomes completely covered by water, and the water film area typically saturates during the second stage. The water film thickness rapidly increases, causing a rapid decrease in the shear strength of the clay-metal interface. In the third stage, the water film thickness at the clay-metal interface approaches saturation, resulting in a gradual decrease in the shear strength as the water content increases. Therefore, as the water content increases or the consistency index decreases, the shear strength of the clay-metal interface initially increases gradually, then decreases rapidly, and finally decreases slowly (Figure 4). The consistency index and normal pressure are factors that influence the area and thickness of the water film. Under the same normal pressure and consistency index, it can be assumed that the area and thickness of the water film between the clay and metal blocks are similar. In this case, the shear strength of the clay-metal interface is determined by the contact angle (θ_1) of the metal block. The uncoated and coated metal block surfaces have contact angles of 62.04° and 85.48°, respectively. The coated metal block surface has a higher contact angle than the uncoated metal block. However, as the contact angle θ_1 increases, the value of $\cos\theta_1$ decreases. Consequently, the adhesion between the coated metal block and clay has a lower strength compared to the uncoated metal block (Figure 5).

5 Conclusion

The shear strength of the clay-metal interface was investigated in relation to the consistency index using the large-scale direct shear test. A comparison was made between the shear strength of the clay-metal interface with coated and uncoated metal blocks. Furthermore, the mechanism of the anti-adhesion coating was further discussed. The main conclusions of the study are as follows:

(1) With an increase in shear displacement, the shear stress between the clay and metal blocks increased rapidly. However, it tended to stabilize after reaching a certain shear displacement magnitude.
(2) As the consistency index increased, the shear strength of the clay-metal interface exhibited a gradual increase, followed by a significant increase, and eventually approached a stabilized state. When the consistency index was less than 0.6, the shear strength of the clay-metal interface was relatively consistent under various normal pressures. However, for consistency indexes higher than 0.6, the shear strength of the clay-metal interface varied significantly under different normal pressures.
(3) The application of the anti-adhesion coating resulted in a decrease in the hydrophilicity of the metal block surface and an increase in the contact angle. Consequently, under the same normal pressure and consistency index, the shear strength between the coated metal block and clay was lower compared to that between the uncoated metal block and clay. This suggests that the anti-adhesion coating has the potential to reduce the occurrence of shield clogging in the adhesive stratum.

This study introduces a novel approach to prevent shield clogging, which involves applying anti-sticking coatings on the surface of the cutter and cutting tools. However, the current research is limited to laboratory experiments, and the specific effectiveness needs further validation through field testing. Other properties of the coatings, such as wear resistance and high-temperature durability, also require further investigation.

Data availability statement

The original contributions presented in the study are included in the article/supplementary material, further inquiries can be directed to the corresponding author.

Author contributions

PL: conceptualization, methodology, investigation, funding acquisition, and formal analysis; SS: resources and supervision; ZY: investigation and writing–original draft; FJ: software, data curation, and writing–review and editing; CX: software; supervision; HZ: validation. All authors contributed to the article and approved the submitted version.

Funding

The financial support from the China Postdoctoral Science Foundation (Grant No. 2022M723536) are acknowledged and appreciated.

Conflict of interest

Authors PL, ZY, JF, and CX were by the CCCC Second Harbor Engineering Company Ltd. Author SS was employed by the CCCC First Harbor Engineering Company Ltd.

The remaining author declares that the research was conducted in the absence of any commercial or financial relationships that could be construed as a potential conflict of interest.

The reviewer CZ declared a shared affiliation with the author HZ to the handling editor at the time of review.

Publisher's note

References

Akiyama, Y., and Yokoi, H. (1972). Study on the adhesion of soil (Part 2): theoretical analysis on the mechanism of adhesive force at the saturated stage. *Jpn. J. Soil Sci. Plant Nutr.* 43, 271–277.

Basmenj, A. K., Ghafoori, M., Cheshomi, A., and Azandariani, Y. K. (2016). Adhesion of clay to metal surface; normal and tangential measurement. *Geomechanics Eng.* 10 (2), 125–135. doi:10.12989/gae.2016.10.2.125

Bircha, R. A., Ekwue, E. I., and Phillip, C. J. (2016). Soil-metal sliding resistance forces of some Trinidadian soils at high water. *West Indian* 38 (2), 52–58. doi:10.1007/978-3-662-48510-1_13

Burbaum, U., and Sass, I. (2017). Physics of adhesion of soils to solid surfaces. *Bull. Eng. Geol. Environ.* 76 (3), 1097–1105. doi:10.1007/s10064-016-0875-5

Cao, L., Zhang, D., and Fang, Q. (2020). Semi-analytical prediction for tunnelling induced ground movements in multi-layered clayey soils. *Tunn. Undergr. Space Technol.* 102, 103446. doi:10.1016/j.tust.2020.103446

Chen, Z., Bezuijen, A., Fang, Y., Wang, K., and Deng, R. (2022). Experimental study and field validation on soil clogging of EPB shields in completely decomposed granite. *Tunn. Undergr. Space Technol.* 120, 104300. doi:10.1016/j.tust.2021.104300

Ding, L., and Xu, J. (2017). A review of metro construction in China: organization, market, cost, safety and schedule. *Front. Eng.* 4, 4–19. doi:10.15302/j-fem-2017015

Eom, S. H., Kim, S. S., and Lee, J. B. (2020). Assessment of anti-corrosion performances of coating systems for corrosion prevention of offshore wind power steel structures. *Coatings* 10 (10), 970. doi:10.3390/coatings10100970

Gao, Y., Yu, Z., Chen, W., Yin, Q., Wu, J., and Wang, W. (2023). Recognition of rock materials after high-temperature deterioration based on SEM images via deep learning. *J. Mater. Res. Technol.* 25, 273–284. doi:10.1016/j.jmrt.2023.05.271

Hollmann, F. S., and Thewes, M. (2013). Assessment method for clay clogging and disintegration of fines in mechanised tunnelling. *Tunn. Undergr. Space Technol.* 37, 96–106. doi:10.1016/j.tust.2013.03.010

Huang, J., Liu, X., Song, D., Zhao, J., Wang, E., and Zhang, J. (2022). Laboratory-scale investigation of response characteristics of liquid-filled rock joints with different joint inclinations under dynamic loading. *J. Rock Mech. Geotechnical Eng.* 14 (2), 396–406. doi:10.1016/j.jrmge.2021.08.014

Huang, P., Guo, D., and Wen, S. (2013). *Interface mechanics*. Beijing: Tsinghua university press.

Jia, B., and Gao, Z. (2022). Investigating surface deformation caused by excavation of curved shield in upper soft and lower hard soil. *Front. Earth Sci.* 10, 844969. doi:10.3389/feart.2022.844969

Langmaack, L., and Lee, K. F. (2016). Difficult ground conditions? Use the right chemicals! Chances–Limits–Requirement. *Tunn. Undergr. Space Technol.* 57, 112–121. doi:10.1016/j.tust.2016.01.011

Li, X., Chen, S., Wang, S., Zhao, M., and Liu, H. (2021). Study on *in situ* stress distribution law of the deep mine taking Linyi Mining area as an example. *Adv. Mater. Sci. Eng.* 9 (4), 5594181–5594211. doi:10.1155/2021/5594181

Li, X., Zhang, X., Shen, W., Zeng, Q., Chen, P., Qin, Q., et al. (2023). Research on the mechanism and control technology of coal wall sloughing in the ultra-large mining height working face. *Int. J. Environ. Res. Public Health* 20 (2), 868. doi:10.3390/ijerph20010868

Li, X., Yang, Y., Li, X., and Liu, H. (2022). Criteria for cutting head clogging occurrence during slurry shield tunneling. *Appl. Sci.* 12, 1001. doi:10.3390/app12031001

Liu, H., Zhang, B., Li, X., Liu, C., Wang, C., Wang, F., et al. (2022). Research on roof damage mechanism and control technology of gob-side entry retaining under close distance gob. *Eng. Fail. Anal.* 138 (5), 106331. doi:10.1016/j.engfailanal.2022.106331

Liu, P., Wang, S., Ge, L., Thewes, M., Yang, J., and Xia, Y. (2018). Changes of Atterberg limits and electrochemical behaviors of clays with dispersants as conditioning agents for EPB shield tunnelling. *Tunn. Undergr. Space Technol.* 73, 244–251. doi:10.1016/j.tust.2017.12.026

Liu, P., Wang, S., Shi, Y., Yang, J., Fu, J., and Yang, F. (2019). Tangential shear strength of the clay-metal interface between clay and steel for various soil softnesses. *J. Material Civ. Eng.* 31 (5), 04019048. doi:10.1061/(ASCE)MT.1943-5533.0002680

Liu, S., Li, X., Wang, D., and Zhang, D. (2020). Investigations on the mechanism of the microstructural evolution of different coal ranks under liquid nitrogen cold soaking. *Energy Sources, Part A Recovery, Util. Environ. Eff.* 2020, 1–17. doi:10.1080/15567036.2020.1841856

Martinelli, D., Peila, D., and Campa, E. (2015). Feasibility study of tar sands conditioning for earth pressure balance tunnelling. *J. Rock Mech. Geotechnical Eng.* 7 (06), 684–690. doi:10.1016/j.jrmge.2015.09.002

Niu, H., Weng, X., Hu, J., and Hou, L. (2022). Centrifugal test and instability model analysis of excavation surface stability of a shield tunnel in a clay layer. *Front. Earth Sci.* 10, 850505. doi:10.3389/feart.2022.850505

Peila, D., Picchio, A., Martinelli, D., and Dal, N. E. (2015). Laboratory tests on soil conditioning of clayey soil. *Acta Geotech.* 11 (5), 1061–1074. doi:10.1007/s11440-015-0406-8

Ren, L., Tong, J., Chen, B., and Wu, L. (1990). Thermodynamic analyses of behavior of soil-solid surface adhesion. *Trans. Chin. Soc. Agric. Mach.* 6 (4), 7–12.

Sass, I., and Burbaum, U. (2009). A method for assessing adhesion of clays to tunneling machines. *Bull. Eng. Geol. Environ.* 68 (1), 27–34. doi:10.1007/s10064-008-0178-6

Song, D., Liu, X., Chen, Z., Chen, J., and Cai, J. (2021). Influence of tunnel excavation on the stability of a bedded rock slope: a case study on the mountainous area in southern anhui, China. *KSCE J. Civ. Eng.* 25, 114–123. doi:10.1007/s12205-020-0831-6

Thewes, M., and Hollmann, F. (2016). Assessment of clay soils and clay-rich rock for clogging of TBMs. *Tunn. Undergr. Space Technol.* 57, 122–128. doi:10.1016/j.tust.2016.01.010

USDA (United States Department of Agriculture) (1938). *Soils and men: yearbook of agriculture*. USA: United States Government Printing Office.

Wang, M., Zhao, D., Lv, Y., Wang, W., and Wang, X. (2023a). Prediction method of shield tunneling parameters in pebble stratum formed by weathered granite and quartzite. *Front. Earth Sci.* 10, 1069924. doi:10.3389/feart.2022.1069924

Wang, N., Jiang, Y., Geng, D., Huang, Z., and Ding, H. (2022a). Numerical investigation of the combined influence of shield tunneling and pile cutting on underpinning piles. *Front. Earth Sci.* 10, 896634. doi:10.3389/feart.2022.896634

Wang, S., Liu, P., Gong, Z., and Yang, P. (2021). Auxiliary air pressure balance mode for EPB shield tunneling in water-rich gravelly sand strata: fasibility and soil conditioning. *Case Stud. Constr. Mater.* 16, e00799. doi:10.1016/j.cscm.2021.e00799

Wang, S., Liu, P., Hu, Q., and Zhong, J. (2020). Effect of dispersant on the tangential adhesion strength between clay and metal for EPB shield tunnelling. *Tunn. Undergr. Space Technol.* 95, 103144. doi:10.1016/j.tust.2019.103144

Wang, S., Liu, P., Zhong, J., Ni, Z., and Qu, T. (2022b). Influence factors and calculation model of the shear strength of the clay-metal interface of clayey soil. *Transp. Saf. Environ.* 4, tdac012. doi:10.1093/tse/tdac012

Wang, S., Zhou, Z., Liu, P., Yang, Z., Pan, Q., and Chen, W. (2023b). On the critical particle size of soil with clogging potential in shield tunneling. *J. Rock Mech. Geotechnical Eng.* 15, 477–485. doi:10.1016/j.jrmge.2022.05.010

Wang, Z., Guo, B., Wei, G., Yao, D., and Hu, C. (2022c). Study for longitudinal deformation of shield tunnel in side of foundation pit based on virtual image technique. *Appl. Sci.* 12, 8745. doi:10.3390/app12178745

Xiao, X., Xia, Y., Mao, X., Wang, Y., Fang, Z., Wang, F., et al. (2020). Effect of the nozzle structure of the large-diameter slurry shield cutterhead on the scouring characteristics. *J. Braz. Soc. Mech. Sci. Eng.* 42, 157. doi:10.1007/s40430-020-2255-0

Xu, C., Zhu, Y., Song, D., Liu, X., Guo, W., and Wang, E. (2022). Spacing optimization of the TBM disc cutter rock fragmentation, based on the Energy entropy method. *Sustainability* 14, 13226. doi:10.3390/su142013226

Xu, L., Wu, C., Wang, L., and Xu, S. (2020). Influence and evaluation of saturated soil shield construction on existing highway. *Transp. Saf. Environ.* 3, 72–83. doi:10.1093/tse/tdaa028

Yang, K., Shi, J., Wang, L., Chen, Y., Liang, C., Yang, L., et al. (2022). Bacterial anti-adhesion surface design: surface patterning, roughness and wettability: a review. *J. Mater. Sci. Technol.* 99, 82–100. doi:10.1016/j.jmst.2021.05.028

Yang, Z., Liu, P., Chen, P., Li, S., and Ji, F. (2023). Clogging prevention of slurry–earth pressure balance dual-mode shield in composed strata with medium–coarse sand and argillaceous siltstone. *Appl. Sci.* 13, 2023. doi:10.3390/app13032023

Zeng, L., Li, F., Liu, J., Gao, Q., and Bian, H. (2020). Effect of initial gravimetric water content and cyclic wetting–drying on soil–water characteristic curves of disintegrated carbonaceous mudstone. *Transp. Saf. Environ.* 1, 230–240. doi:10.1093/tse/tdz018

Zhang, L., Ren, L., Tong, J., and Shi, Y. (2004). Study of soil-solid adhesion by grey system theory. *Prog. Nat. Sci.* 14 (2), 119–124. doi:10.1080/10020070412331343241

Zhang, Y., Yan, G., You, K., and Fang, F. (2020). Study on α-Al_2O_3 anti-adhesion coating for molds in precision glass molding. *Surf. Coatings Technol.* 391, 125720. doi:10.1016/j.surfcoat.2020.125720

Zhou, X., Wang, S., Li, X., Meng, J., Li, Z., Zhang, L., et al. (2022). Research on theory and technology of floor heave control in semicoal rock roadway: taking longhu coal mine in Qitaihe mining area as an Example. *Lithosphere* 2022 (11), 3810988. doi:10.2113/2022/3810988

Zumsteg, R., and Langmaack, L. (2017). Mechanized tunneling in soft soils: choice of excavation mode and application of soil-conditioning additives in glacial deposits. *Engineering* 3 (06), 863–870. doi:10.1016/j.eng.2017.11.006

Zumsteg, R., Ploetze, M., and Puzrin, A. (2013). Reduction of the clogging potential of clays: new chemical applications and novel quantification approaches. *Geotechnique* 63 (4), 276–286. doi:10.1680/geot.sip13.p.005

Zumsteg, R., and Puzrin, A. M. (2012). Stickiness and adhesion of conditioned clay pastes. *Tunn. Undergr. Space Technol.* 31 (5), 86–96. doi:10.1016/j.tust.2012.04.010